Scripta Materialia 131 (2017) 29–32

Contents lists available at ScienceDirect

Scripta Materialia

journal homepage: www.elsevier.com/locate/scriptamat

Regular Article

In situ synchrotron investigation of grain growth behavior of nano-grained UO_2

Yinbin Miao[a], Tiankai Yao[b], Jie Lian[b], Jun-Sang Park[a], Jonathan Almer[a], Sumit Bhattacharya[c], Abdellatif M. Yacout[a], Kun Mo[a,*]

[a] *Argonne National Laboratory, Lemont, IL60439, United States*
[b] *Rensselaer Polytechnic Institute, Troy, NY12180, United States*
[c] *Northwestern University, Evanston, IL60208, United States*

ARTICLE INFO

Article history:
Received 24 October 2016
Received in revised form 12 December 2016
Accepted 16 December 2016
Available online 9 January 2017

Keywords:
X-ray diffraction
Synchrotron radiation
Grain growth
Nanocrystalline materials
Uranium dioxide

ABSTRACT

The study of grain growth kinetics in nano-grained UO_2 samples is reported. Dense nano-grained UO_2 samples with well-controlled stoichiometry and grain size were fabricated using the spark plasma sintering technique. To determine the grain growth kinetics at elevated temperatures, a synchrotron wide-angle X-ray scattering (WAXS) study was performed *in situ* to measure the real-time grain size evolution based on the modified Williamson-Hall analysis. The unique grain growth kinetics of nanocrystalline UO_2 at 730 °C and 820 °C were observed and explained by the difference in mobility of various grain boundaries.

A nano-grained structure with microscale intergranular pores, known as the high burnup structure (HBS), forms in the rim region of UO_2 fuel pellets at high burnup (beyond approximately 50 GWd/tU)[1,2]. During the formation of the HBS, the initially micron-sized UO_2 grain structures develop into 100–300 nm sized grains by grain subdivision/recrystallization. The HBS has different material properties due to its nanocrystalline nature, such as recovered thermal conductivity[3] and enhanced radiation tolerance. The appearance of the HBS, therefore, alters the fuel performance of UO_2, by changing its thermophysical properties and fission gas behavior. The HBS evolution is believed to be a consequence of the competition between radiation-induced grain subdivision/recrystallization and grain growth driven by both elevated temperatures and radiation. While the grain growth kinetics of UO_2 with conventional grain size (on the order of 10 μm) have been systematically investigated and well understood[4–6], little is known about the nano-grained UO_2 formed in the HBS. Previous studies indicate that the grain growth mechanism and kinetics of nanocrystalline materials can differ significantly from those in conventional materials[7–9]. Therefore, understanding the microstructure evolution of nanocrystalline UO_2 is essential to develop a better understanding of the fuel performance of UO_2 at high burnup. This knowledge will facilitate further development of advanced fuel performance codes like MARMOT[10]. These codes are ultimately expected to predict the fuel performance of UO_2 with high credibility.

While *ex situ* grain growth investigations can only sample limited data points during isothermal annealing, *in situ* grain growth investigations are capable of capturing detailed kinetics by monitoring real-time grain size evolution for prospective mechanism analysis and model development. However, *in situ* grain growth investigation requires high-frequency non-destructive grain size measurement that does not interrupt the continuous isothermal annealing. As the microstructural information including grain size is contained in diffraction signals, synchrotron wide-angle X-ray scattering (WAXS) was utilized in this study to measure the grain size based on the modified Williamson-Hall (W-H) analysis[11]. This technique and analysis method have been successfully applied to measure the grain size or dislocation density in a variety of nuclear structural materials[12–16] and nuclear fuels[17].

The nano-grained samples used in this study were synthesized at 700 °C using the spark plasma sintering (SPS) technique. Since the as-sintered samples were hyper-stoichiometric, they were reduced in a hydrogen environment at 600 °C to recover their stoichiometry.

* Corresponding author at: 9700 S. Cass Ave, Lemont, IL60439, United States.
E-mail address: kunmo@anl.gov (K. Mo).

http://dx.doi.org/10.1016/j.scriptamat.2016.12.025
1359-6462/

The stoichiometry after reduction was determined to be $UO_{2.006\pm0.002}$ based on the lattice constant[18] measured by a PANalytical X'Pert PRO diffractometer. The porosity of the samples is 3.5% and the grain size is 120±5 nm, according to scanning electron microscopy (SEM) images of the fracture surface (Fig. 4 (a)). A high-temperature and high-vacuum apparatus was built to carry out the grain growth investigation. The approximately 10 mm × 10 mm × 0.5 mm specimen was wrapped in double layers of 10 μm Ni foil and fastened between stainless steel (SS) frames to isolate the radiation hazard. The entire sample holder was further encapsulated in a quartz dome to form a vacuum chamber. The vacuum prevents UO_2 from being further oxidized to hyper-stoichiometry or even U_4O_9/U_3O_7 or U_3O_8 at elevated temperatures[19]. The use of Ni foil also helps absorb any residual oxygen. The sample holder is located in the top part of the quartz dome and can be heated to 1000 ° C by an infrared clamp furnace. Four K-type thermocouples are attached to the corners of the stainless steel frames to control and monitor the sample temperature. The high-energy synchrotron WAXS experiment was carried out at Sector 1-ID Hutch E at the Advanced Photon Source (APS), Argonne National Laboratory (ANL). Diffraction measurements were performed with a monochromatic 78.4 keV ($\lambda = 0.1581$ Å) or 90.6 keV ($\lambda = 0.1368$ Å) X-ray beam with a beam size of 50 μm × 50 μm. The "Hydra" detector array, which consists of four GE 41RT area detectors, was used to collect the diffraction signals. The detailed experiment setup is shown in Fig. 1.

The nano-grained UO_2 samples were heated to two target temperatures, 750 °C and 815 °C, at a rate of 60 ° C/min. The temperature overshoot was less than 5 °C. After the target temperatures were achieved, the specimens were isothermally annealed for approximately 7.5 h. Because the thermocouples are still millimeters away from the specimens, the specimen temperatures were calibrated using the thermal expansion of the UO_2 lattice[20]. The actual specimen temperatures, based on ther lattice constant calibration, were

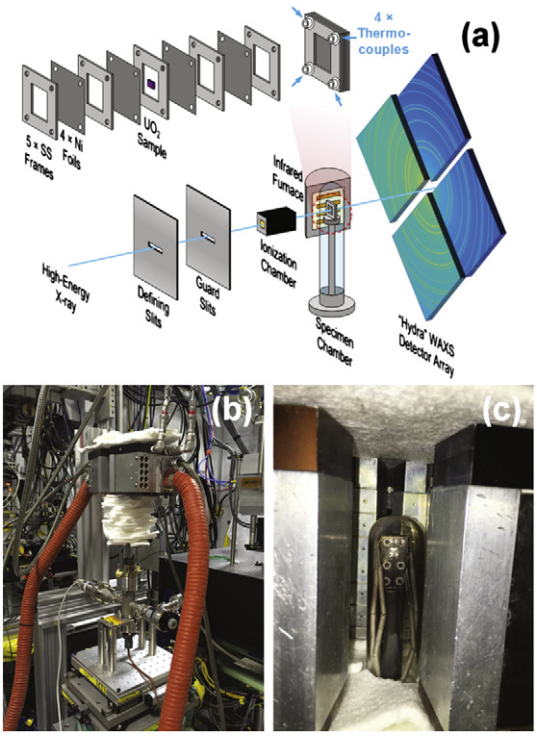

Fig. 1. The experimental setup of the *in situ* synchrotron X-ray grain growth study of nano-grained UO_2: (a) schematic showing the sample holder, vacuum chamber, and synchrotron experimental setup; (b) the vacuum chamber installed in the Sector 1-ID Hutch E at APS; (c) a close-up of the sample holder encapsulated in the vacuum chamber.

730 °C and 820 °C, respectively. The specimen temperatures were quite stable (variations were less than ±5°C) during the experiment. WAXS exposures of the UO_2 specimens were taken once every 9 s. The diffraction peaks collected by the Hydra detector array were each fit to a pseudo-Voigt function to obtain their breadths. The modified W-H analysis was then utilized to measure the evolution of grain size. In the modified W-H analysis, the broadening of the diffraction peaks is interpreted as follows:

$$\Delta K = \frac{0.9}{D} + \left(\frac{\pi A^2 b^2}{2}\right)^{\frac{1}{2}} \rho^{\frac{1}{2}} \left(K\bar{C}^{\frac{1}{2}}\right), \tag{1}$$

where D is the grain size, A is an adjustable parameter that was selected to be 1 in this study assuming a dislocation density on the order of 10^{14} m^{-2}, b is the length of the Burgers vector, ρ is the dislocation density, $\bar{C}$ is the contrast factor, $K = 2sin\theta/\lambda$, and $\Delta K = 2cos\theta\Delta\theta/\lambda$, θ is the diffraction angle, $\Delta\theta$ is the peak breadth, and λ is the wavelength of the X-ray photons. The dislocation density in nanocrystalline UO_2 is likely to be less than 10^{14} m^{-2}. However, the selection of A does not influence the deduction of grain size, D. Because dislocation density measurement is not the focus of this study, the value of A was not intentionally optimized. $\bar{C}$ is a material property. The temperature-dependent $\bar{C}$ was calculated according to Ungar's method[21]:

$$\bar{C} = \bar{C}_{h00}(1 - qH^2), \tag{2}$$

where $\bar{C}_{h00}$ is the average contrast factor of {h00} reflections, q is a material-dependent parameter, and H^2 is a reflection parameter determined by {hkl}. Both $\bar{C}_{h00}$ and q are determined by the crystal structure and single crystal elastic stiffness tensor. As the values of $\bar{C}_{h00}$ and q contributed by edge (subscript e) and screw (subscript s) dislocations are different, $\bar{C}$ has the following expression when both types of dislocations coexist:

$$\bar{C} = \left[\nu_s \bar{C}_{h00,s} + (1-\nu_s)\bar{C}_{h00,e}\right]\left\{1 - [\nu_s q_s + (1-\nu_s)q_e]H^2\right\}, \tag{3}$$

where ν_s is the fraction of screw dislocations. During the linear regression of Eq. (1), ν_s was optimized by maximizing the coefficient of determination (r^2). $\bar{C}_{h00}$ and q of both edge and screw dislocations were deduced from the stiffness tensors at various temperatures measured by inelastic neutron scattering[22], and are listed in Table 1. In order to validate the *in situ* measured grain size, an as-sintered specimen and the two annealed specimens were measured using SEM to determine their grain sizes.

The diffraction line profile of the as-sintered UO_2 specimen (the black curve in Fig. 2) shows a perfect powder diffraction pattern from the nano-grained UO_2 phase. Also observed were the diffraction peaks from the Ni foils. As the {331} reflection of UO_2 is very close to the {220} reflection of Ni, only eight UO_2 reflections ({111}, {200}, {220}, {311}, {222}, {400}, {420}, and {422}) were used in the modified W-H analysis. No additional diffraction peaks (from other

Table 1
The parameters used in the calculation of the contrast factors.

Parameter	730 ° C	820 ° C
C_{11} (GPa)[22]	335.0	328.0
C_{12} (GPa)[22]	112.5	111.1
C_{44} (GPa)[22]	59.4	58.6
$A = 2C_{44}/(C_{11} - C_{12})$	0.534	0.540
C_{12}/C_{44}	1.894	1.896
$\bar{C}_{h00,s}$	0.1235	0.1241
$\bar{C}_{h00,e}$	0.1390	0.1396
q_s	−0.3186	−0.2952
q_e	−1.4157	−1.3922

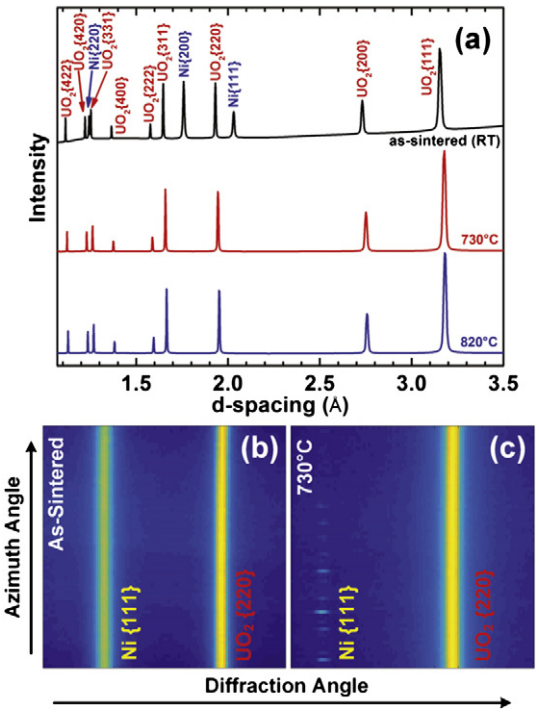

Fig. 2. The synchrotron diffraction data from as-received and isothermally annealed UO_2 specimens: (a) azimuthally integrated diffraction peaks of the as-sintered specimen (taken at room temperature) as well as specimens annealed at 730 °C and 820 °C for approximately 7.5 h (taken at annealing temperatures); (b)/(c) 2D diffraction data focusing on the {220} reflection of UO_2 and the {111} reflection of Ni, showing that the grain growth in the Ni foil results in the fading of its Debye-Schurrer diffraction rings.

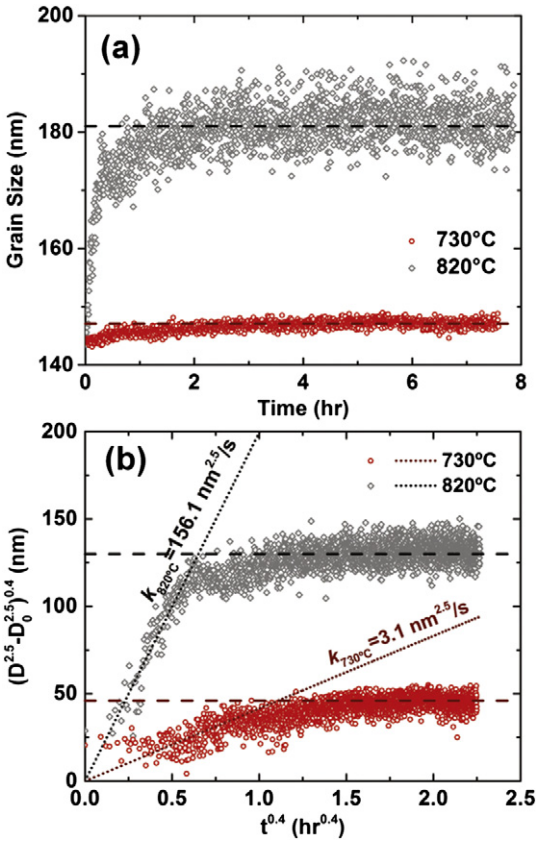

Fig. 3. The grain growth kinetics measured by in situ synchrotron X-ray diffraction based on the modified Williamson-Hall analysis: (a) the grain size evolution over the 7.5-h isothermal annealing; (b) the initial growth stage fitted to the grain growth model.

phases) appeared after 7.5 h annealing, as shown by the red and blue curves in Fig. 2. The lattice parameter of UO_2 also remained stable throughout the isothermal annealing. This demonstrates that the vacuum chamber prevented further oxidation of the UO_2. Additionally, the grain growth in Ni foils was quite prominent. That is, the Debye-Scherrer rings from Ni turned into separate diffraction spots (Fig. 2 (b) and (c)) and therefore faded on the azimuthally-integrated diffraction line profile shown in Fig. 2 (a).

The modified W-H analysis shows that the grain size of the UO_2 specimens before isothermal annealing is 144±1 nm. Annealed at 820 ° C, the grain size increases to approximately 181±6 nm within the first two hours. After this initial rapid growth stage, no significant change in grain size was observed in the following 5.5 h (Fig. 3). On the other hand, the grain growth at 730 °C is moderate. The grain size was found to slightly increase to 147±2 nm and then remain at this size through the remainder of the isothermal annealing (Fig. 3). To validate the grain size measurement based on the synchrotron WAXS techniques, SEM was performed to measure the grain sizes on the fracture surfaces of the isothermally annealed specimens, shown in Fig. 4 (b) and (c). The grain sizes of the UO_2 samples annealed at 730 °C and 820 °C were respectively measured to be 127±5 nm and 148±7 nm according to the SEM measurement.

In comparing the grain sizes determined by synchrotron and SEM analysis (Table 2), the synchrotron-measured grain sizes are always larger than the SEM-deduced values. This difference stems from the fact that the SEM images are actually 2D-projected observations only focused on cross-section surfaces, whereas the synchrotron technique measures the true 3D grain structure. Assuming a spherical grain shape, the 3D and 2D grain sizes theoretically differ by a factor of $\sqrt{3/2}$, or approximately 1.22, which agrees well with the ratios obtained in this study (Table 2). The grain sizes measured by synchrotron diffraction are therefore consistent with the SEM measurements. This comparison also demonstrates that synchrotron X-ray diffraction can accurately measure the grain size of nanocrystalline materials with equiaxed grains.

In situ synchrotron measurement provided detailed two-stage grain size evolution, wherein the majority of the grain growth took place in the first two or three hours of annealing time; after the initial growth, the grain structure was stabilized at the annealing temperature with no significant increase in grain size. Assuming an empirical UO_2 grain growth model [6]: $D^{2.5} - D_0^{2.5} = kt$, where D is the grain size, D_0 is the initial grain size, k is the grain boundary mobility, and t is the annealing time, the $(D^{2.5} - D_0^{2.5})^{0.4}$ vs. $t^{0.4}$ diagram of the *in situ* grain growth data was illustrated in Fig. 3 (b). It is clear that the measured grain growth kinetics at both temperatures fit the model well in the initial stage of isothermal annealing (approximately half an hour for the 820 °C and an hour for the 730 °C annealing), yielding grain boundary mobility of 156.1 $nm^{2.5}/s$ and 3.1 $nm^{2.5}/s$, respectively (compared to 2.09×10^{-2} $nm^{2.5}/s$ and 8.88×10^{-4} $nm^{2.5}/s$ as predicted by Hastings et al.'s empirical formula for UO_2 with micron-sized grains[6]). Beyond the initial stage, the grain growth kinetics slows down and deviates from the model prediction. After approximately two hours at 820 ° C or three hours at 730 °C, the grain growth almost ceases. The stagnation of grain growth observed in this study can be explained by the mechanism discovered by Holm and Foil[7]. Each type of grain boundary has a characteristic temperature, T_c, at which the grain boundaries transition from low-mobility to high-mobility. The characteristic temperatures can vary by a considerable amount due to the variation in activation energy of different types of grain boundaries[23]. Namely, at a specific temperature, T, only those grain boundaries with $T_c < T$ have high-mobility

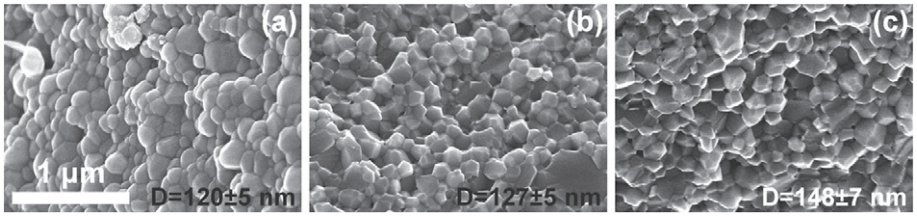

Fig. 4. SEM images of the fracture surfaces of (a) the as-sintered sample, (b) the sample annealed at 730 ° C for approximately 7.5 h, and (c) the sample annealed at 820 ° C for approximately 7.5 h. The intergranular fracture surfaces were used for *ex situ* grain size measurement.

and therefore contribute effectively to grain growth. During this process, the high-mobility grain boundaries are consumed, leaving the low-mobility grain boundaries ($T_c > T$) in the system. Therefore, the grain growth decelerates after the initial stage and eventually arrives at stagnation. As a result, there is a saturation grain size at each isothermal annealing temperature.

The nano-grained UO_2 sample was sintered at 700 °C and reduced at 600 °C. The grain boundaries with T_c lower than 600 °C were eliminated during the reduction, while some of those grain boundaries with 600 °C$\leq T_c \leq$ 700°C may still survive the fabrication due to the non-equilibrium nature of SPS manufacturing. The initial grain size can then be regarded as the saturation grain size at a temperature slightly lower than 700 °C. Hence, the grain growth at only 30 °C above the sintering temperature is marginal. On the other hand, when the annealing temperature increases to 820 °C, a considerable number of grain boundaries are activated, leading to prominent grain growth. Additionally, due to the lower sintering temperature of the nano-grained UO_2 sample, more low-T_c grain boundaries exist in the system. Thus, the grain growth kinetics of nano-grained UO_2 are not comparable to those of conventional micro-grained UO_2 (usually sintered at over 1500 °C [24,25]). During the formation of the HBS, radiation-induced grain subdivision/recrystallization may also create numerous grain boundaries with low T_c. Thus, the grain growth kinetics and stagnation mechanism observed in this study will expand the understanding of the microstructure evolution of nano-grained UO_2 as identified in the HBS, enlightening the future study of the characteristics of the HBS and supporting the development of advanced fuel performance code. In addition, a series of factors, such as porosity, initial grain size, and stoichiometry, are expected to influence grain growth kinetics of nano-grained UO_2. With the capability of *in situ* synchrotron grain growth measurement established in this study, systematic experimental investigations on the effects of these aforementioned factors have been planned.

In this study, the grain growth behavior of stoichiometric nanocrystalline UO_2 was investigated through *in situ* synchrotron radiation experiments. The unique grain growth kinetics of nanocrystalline UO_2 were observed and explained by the mobility difference of various grain boundaries. The grain growth behavior of nanocrystalline UO_2 sheds light on the microstructure evolution of the HBS and therefore provides a valuable reference for the validation of models used in the MARMOT code.

This work was funded by the Fuel Product Line (FPL) in the U.S. Department of Energy (DOE) 's Nuclear Energy Advanced Modeling and Simulation (NEAMS) program and the U.S. DOE's Nuclear Energy University Program (NEUP) DE-NE0008440. This research used resources of the Advanced Photon Source, a U.S. DOE Office of Science User Facility operated for the DOE Office of Science by Argonne National Laboratory under contract no. DE-AC-02-06CH11357 between UChicago Argonne, LLC and the U.S. Department of Energy. This work made use of the EPIC facility (NUANCE Center-Northwestern University), which has received support from the MRSEC program (NSFDMR-1121262) at the Materials Research Center; the Nanoscale Science and Engineering Center (NSFEEC-0647560) at the International Institute for Nanotechnology; and the State of Illinois, through the International Institute for Nanotechnology.

Table 2
Comparison of the grain sizes measured by synchrotron and SEM techniques.

Sample	Synchrotron	SEM	Ratio
As-received	144±1 nm	120±5 nm	1.20
730 ° annealed	147±2 nm	127±5 nm	1.16
820 ° annealed	181±6 nm	148±7 nm	1.22

References

[1] H. Matzke, J. Spino, J. Nucl. Mater. 248 (1997) 170–179.
[2] V.V. Rondinella, T. Wiss, Mater. Today 13 (2010) 24–32.
[3] C. Ronchi, M. Sheindlin, D. Staicu, M. Kinoshita, J. Nucl. Mater. 327 (2004) 58–76.
[4] I. Amato, R. Colombo, A.P. Balzari, J. Nucl. Mater. 18 (1966) 252–260.
[5] J. Ainscough, B. Oldfield, J. Ware, J. Nucl. Mater. 49 (1973) 117–128.
[6] I. Hastings, J. Scoberg, K. MacKenzie, J. Nucl. Mater. 82 (1979) 435–438.
[7] E.A. Holm, S.M. Foiles, Science 328 (2010) 1138–1141.
[8] R. Calinas, M. Vieira, M. Vieira, P. Ferreira, et al. Nanotechnology 21 (2010) 145701.
[9] D.S. Aidhy, Y. Zhang, W.J. Weber, Scr. Mater. 83 (2014) 9–12.
[10] M.R. Tonks, D. Gaston, P.C. Millett, D. Andrs, P. Talbot, Comput. Mater. Sci. 51 (2012) 20–29.
[11] T. Ungár, Materials Science Forum, vol. 278, Trans Tech Publ. 1998, pp. 151–157.
[12] Y. Miao, K. Mo, Z. Zhou, X. Liu, K.-C. Lan, G. Zhang, M.K. Miller, K.A. Powers, J. Almer, J.F. Stubbins, Mater. Sci. Eng. A 625 (2015) 146–152.
[13] Y. Miao, K. Mo, Z. Zhou, X. Liu, K.-C. Lan, G. Zhang, M.K. Miller, K.A. Powers, Z.-G. Mei, J.-S. Park, et al. Mater. Sci. Eng. A 639 (2015) 585–596.
[14] G. Zhang, Z. Zhou, K. Mo, Y. Miao, X. Liu, J. Almer, J.F. Stubbins, J. Nucl. Mater. 467 (2015) 50–57.
[15] Y. Miao, K. Mo, Z. Zhou, X. Liu, K.-C. Lan, G. Zhang, J.-S. Park, J. Almer, J.F. Stubbins, Mater. Des. 111 (2016) 622–630.
[16] J.-L. Lin, K. Mo, D. Yun, Y. Miao, X. Liu, H. Zhao, D.T. Hoelzer, J.-S. Park, J. Almer, G. Zhang, et al. J. Nucl. Mater. 471 (2016) 289–298.
[17] Y. Miao, K. Mo, B. Ye, L. Jamison, Z.-G. Mei, J. Gan, B. Miller, J. Madden, J.-S. Park, J. Almer, et al. Scr. Mater. 114 (2016) 146–150.
[18] K. Teske, H. Ullmann, D. Rettig, J. Nucl. Mater. 116 (1983) 260–266.
[19] G. Rousseau, L. Desgranges, F. Charlot, N. Millot, J. Niepce, M. Pijolat, F. Valdivieso, G. Baldinozzi, J. Bérar, J. Nucl. Mater. 355 (2006) 10–20.
[20] I.A.E. Agency, Thermophysical properties database of materials for light water reactors and heavy water reactors, International Atomic Energy Agency. 2006,
[21] T. Ungár, I. Dragomir, Á. Révész, A. Borbély, J. Appl. Crystallogr. 32 (1999) 992–1002.
[22] M.T. Hutchings, J. Chem. Soc. Faraday Trans. 2 83 (1987) 1083–1103.
[23] D.L. Olmsted, E.A. Holm, S.M. Foiles, Acta Mater. 57 (2009) 3704–3713.
[24] G. Bandyopadhyay, J. Roberts, J. Am. Ceram. Soc. 59 (1976) 415–419.
[25] S. Coleman, W. Beere, Philos. Mag. 31 (1975) 1403–1413.